Journal of Power Sources 242 (2013) 877–883

Contents lists available at SciVerse ScienceDirect

Journal of Power Sources

journal homepage: www.elsevier.com/locate/jpowsour

The importance of water transport on short-side chain perfluorosulfonic acid membrane fuel cells operating under low relative humidity

Nana Zhao [a], Dave Edwards [a], Chao Lei [b], Keping Wang [b], Jing Li [b], Yongming Zhang [c], Steven Holdcroft [a,d,*], Zhiqing Shi [a,*]

[a] Energy, Mining and Environment Portfolio, National Research Council Canada, 4250 Wesbrook Mall, Vancouver, British Columbia, Canada V6T 1W5
[b] Automotive Fuel Cell Cooperation Corp., 9000 Glenlyon Parkway, Burnaby, British Columbia, Canada V5J 5J8
[c] School of Chemistry and Chemical Technology, Shanghai Jiao Tong University, 800 Dongchuan Road, Shanghai 200240, China
[d] Department of Chemistry, Simon Fraser University, Burnaby, British Columbia, Canada V5A 1S6

HIGHLIGHTS

- Short-side chain PFSA ionomer membranes provided higher fuel cell performance than NRE-211 at 80 °C and 30% RH.
- A higher water flux through the membrane leads to a higher fuel cell performance.
- Rates of water permeation and effective proton mobility are related.
- Increasing a PFSA membrane's IEC does not always improve fuel cell performance.

ARTICLE INFO

Article history:
Received 21 November 2012
Received in revised form
28 March 2013
Accepted 23 May 2013
Available online 8 June 2013

Keywords:
Fuel cell
PEM
PFSA
Ionomer
Water permeation
Proton conductivity

ABSTRACT

Polarization curves of fuel cells incorporating PFSA short-side chain (SSC) ionomer membranes having ion exchange capacity (IEC) 1.30, 1.37, 1.43 and 1.50 meq g^{-1} and NRE-211 are compared. Under low humidity conditions, fuel cells incorporating SSC membranes show higher performance than NRE-211. SSC PFSA membranes possessing an IEC of 1.37 meq g^{-1} exhibit the highest performance. Differences in fuel cell polarization curves are due to differences in the high frequency resistance, which in turn is found related to ex-situ measurements of both the effective proton mobility and the rate of water flux through the membrane, which also exhibit a maximum for membranes of IEC 1.37 meq g^{-1}. Water permeation and proton mobility are shown to be inherently linked, but it is found that simply increasing the membrane's IEC does not necessarily translate to increased water transport and effective proton mobility, despite the increased water content.

1. Introduction

Proton exchange membrane fuel cells (PEMFCs) are considered an alternative energy conversion technology for vehicular applications to complement the internal combustion engine. The proton-conducting membrane is a key component in this technology as it serves as both the conductor of protons and separator of electrodes and reactant gases. The archetypal membrane is based on a perfluorosulfonic acid (PFSA) ionomer, such as Nafion® [1], which consists of a hydrophobic polytetrafluoroethylene backbone and perfluorovinyl ether side chains terminated by a triflic acid group ($-CF_2SO_3H$). Although Nafion possesses many desirable attributes, it has the recognized limitation of insufficient proton conductivity under low humidity [2]. The short-side chain (SSC) version of PFSA, bearing a $-OCF_2CF_2SO_3H$ pendant chain, has gained recent attention due to its higher degree of crystallinity and thermal resistance [3]. Tant et al. [4,5] and Moore and Martin [6] have previously highlighted a few of the differences between short- and long-side chain PFSA analogs. In the mid-1980s Ballard Power Systems demonstrated significant improvements in fuel cell

* Corresponding authors. Energy, Mining and Environment Portfolio, National Research Council Canada, 4250 Wesbrook Mall, Vancouver, British Columbia, Canada V6T 1W5. Tel.: +1 604 221 3000; fax: +1 604 221 3001.
E-mail addresses: holdcrof@sfu.ca (S. Holdcroft), ken.shi@nrc-cnrc.gc.ca, shi_ken@hotmail.com (Z. Shi).

0378-7753/$ – see front matter © 2013 Crown Copyright and Elsevier Inc. All rights reserved.
http://dx.doi.org/10.1016/j.jpowsour.2013.05.176

performance using SSC membranes produced by Dow Chemical Co. [7].

Over the past decade simpler synthetic routes for producing SSC PFSA ionomer have emerged and several properties of these materials have been reported [8–14]. For example, Solvay Solexis [15] produces and markets Hyflon/Aquivion Ion membranes, reporting higher conductivity, similar mechanical properties, and higher ionic glass-transition temperatures with respect to Nafion. Ghielmi et al. [16] examined the water uptake of extruded, high IEC Hyflon 670 (IEC 1.49 meq g^{-1}) and 770 (IEC 1.30 meq g^{-1}) at 100 °C and reported much larger water uptakes compared to lower IEC analogs. Molecular modeling studies revealed that the hydronium ion diffusion coefficient in SSC PFSA membranes increases with water content [17]. Aricò et al. [13] found that Aquivion™-based MEAs in fuel cell stacks were able to sustain a higher temperature operation than Nafion-based cells. In previous publications, we described the results of fuel cell studies using high IEC, SSC PFSA ionomers as the proton-conducting medium dispersed in the catalyst layer [18,19]. Larger current densities were observed at elevated temperature and under lower relative humidity, compared to Nafion NR211.

Whereas a distinct advantage of SSC PFSA membranes has been demonstrated in fuel cells, a comprehensive understanding of the correlations between water permeation, proton conductivity, and fuel cell performance is not-so-well documented. A greater understanding of the role of transport properties in such materials is essential to optimize and improve fuel cell performance. This is because during fuel cell operation water is transported by electro-osmotic drag from anode to cathode and by back diffusion due to a water concentration gradient and diffusion-driven by pressure gradient [20,21]. Too little water in either the membrane or catalyst layer increases the ionic cell resistance, but too much causes flooding of the catalyst layer which suppresses the transport of gaseous reactants [22–24].

In the present work, fuel cell polarization performance data and water transport properties of short-side chain (SSC) PFSA membranes are studied under comparable conditions of temperature and relative humidity. SSC PFSA ionomers possessing IECs of 1.30, 1.37, 1.43 and 1.50 meq g^{-1} were provided by Dongyue [25,26]. In contrast to our previous studies on SSC PFSA ionomer membranes in which membranes were cast from relatively high boiling point solvents (e.g., DMF) [26], we developed a solution casting process using alcoholic solutions in order to promote “greening” of the membrane fabrication process.

2. Experimental and materials

2.1. Membranes

Short-side chain PFSA ionomer was synthesized and provided by Dongyue as described previously [25,26]. PFSA ionomers possessed an IEC (equivalent weight, EW) of 1.30 (770), 1.37 (730), 1.43 (699) and 1.50 meq g^{-1} (670 g eq^{-1}), as determined by titration 5–15 wt% PFSA ionomer solutions/dispersions were prepared using a mixture of ethanol, 1-propanol, ethylene glycol, and water (26:45:4:25 vol%). Membranes were cast onto a PTFE sheet using a doctor blade, dried at room temperature overnight, and annealed in a vacuum oven at 180 °C for 20 min. As pre-treatment, membranes were heated to 65 °C in 1.0 M sulfuric acid solution for 2 h, rinsed in de-ionized Milli-Q water (Millipore) several times and dried prior to use. For the purpose of this work, membranes are named SSC-1.30, SSC-1.37, SSC-1.43, SSC-1.50. Nafion® membrane (NRE-211, DuPont) was used as received. The fully hydrated thicknesses of SSC-1.30, SSC-1.37, SSC-1.43, SSC-1.50 and NRE-211 were 28 μm, 24 μm, 23 μm, 24 μm and 28 μm, respectively.

2.2. Fabrication of membrane–electrode-assemblies (MEAs)

Catalyst inks were prepared using a dispersion media mixture of 1:1 MeOH/water and 46 wt% Pt/C (Tanaka Kikinzoku Kogyo). The content of Nafion® ionomer in the catalyst layer was 30 wt%. The solids content of the inks was ~1 wt%. An automated spray coater (EFD Ultra TT series) was used to deposit the anode CL (0.2 mg Pt cm^{-2}) and the cathode CL (0.4 mg Pt cm^{-2}) directly onto the membrane. The catalyst-coated membranes (CCMs) possessed an electrode geometrical surface area of 5 × 5 cm^2. Detailed fabrication procedures have been previously described [19,27].

2.3. Single cell assembly and fuel cell testing protocol

Catalyst-coated membranes (CCMs) were sandwiched between sheets of two-layer gas diffusion layers (GDL, SIGRACET 24BC, SGL Carbon Group) and assembled into 25 cm^2 single cells possessing straight flow channels (Fuel Cell Technologies). Single cells were tested in a fuel cell test station (100 W, Scribner 850e, Scribner Associates Inc.), using hydrogen (2 L min^{-1}) and air (5 L min^{-1}) with no back pressure. The cells were conditioned for at least 6 h at 1 A cm^{-2} under 100% RH at 80 °C.

The electrochemical surface area (ECSA) of cells was measured by cyclic voltammetry (CV) using a potentiostat (1287A, Solartron Analytical) operated at a sweep rate of 50 mV s^{-1}. Humidified hydrogen (0.5 SLPM) was fed to the anode, which operated as both counter and reference electrode, while humidified nitrogen (0.5 SLPM) was fed to the cathode (working electrode). After 15 min of purging, the N_2 flow was set to zero, and the cell was stabilized for 15 min. The ECSA was calculated from the integrated charge corresponding to the Pt–H desorption and adsorption peaks. The double-layer capacitance of the cathode catalyst layers (CCLs) was also obtained from the cyclic voltammograms. The errors reported are based on multiple (3) measurements.

2.4. Water content

Hydrated membrane volumes, V_{hyd}, were calculated by assuming that the volume change upon absorption is due to the volume of water incorporated, V_{water}. The latter was calculated from the difference between the weight of the hydrated membrane, W_{hyd}, and the dry weight, W_{dry}, and dividing by the density of water, ρ_{water} (1.0 g mL^{-1}).

$$V_{water} = \frac{W_{hyd} - W_{dry}}{\rho_{water}} \quad (1)$$

The water content, as a volume percentage, X_v, is expressed according to the following relationship:

$$\text{water content(vol\%)} = X_v = \frac{V_{water}}{V_{hyd}} 100\% \quad (2)$$

The acid concentration was determined according to:

$$[-SO_3H] = \frac{\text{moles of } -SO_3H}{V_{hyd}} \quad (3)$$

where $[-SO_3H]$ is the concentration of bound sulfonic acid; moles of $-SO_3H$, was calculated from the IEC and dry mass of the polymer; and V_{hyd} is the hydrated volume of the membrane.

2.5. Proton conductivity and proton mobility

In-plane conductivity measurements were performed using a 2-probe PTFE cell. Membranes were sandwiched between two Teflon

blocks and held in place with nylon screws. An open window in the Teflon block allowed for exposure of the membrane to the environment. The conductivity values were extracted from electrochemical impedance spectra acquired on a Solartron SI1260 Impedance/Gain Phase Analyzer. Conductivity values were measured after a minimum of 1 h of equilibration in water. The extracted ionic resistance was used to calculate proton conductivity (σ_{H^+}), according to the following relationship (Eq. (4)):

$$\sigma_{H^+} = \frac{L}{R_m A} \quad (4)$$

where L is the spacing between the Pt electrodes (1.0 cm); A, the cross-sectional area of the membrane; and R_m, the ionic resistance of the membrane. Details of this procedure have been described previously [28]. The errors reported are based on multiple (3) measurements.

2.6. Ex-situ measurement of water transport through membranes

To obtain liquid–vapor permeation (LVP) data, the membranes were exposed to liquid water on one side and water vapor with controlled RH on the other side, according to Fig. 1. The measurement process and calibrations required have been described in detail previously [29,30]. Briefly, a membrane was floated on the surface of water in a stainless steel container and placed in the environmental chamber such that one side of the membrane is exposed to liquid water, while the other side is exposed to water vapor with a RH controlled by the environmental chamber. In this study, the RH of the environmental chamber, and thus the vapor above the membrane was varied from 30% to 80% RH at 80 °C. The container containing water and membrane was removed from the environmental chamber periodically and weighed. The initial weight of the container was determined after the temperature of the container had stabilized at 80 °C, which typically took 2 h. The mass change of the container was determined at intervals of 1.5–3 h. Rates of liquid–vapor permeation (LVP) were calculated as water fluxes through the membrane.

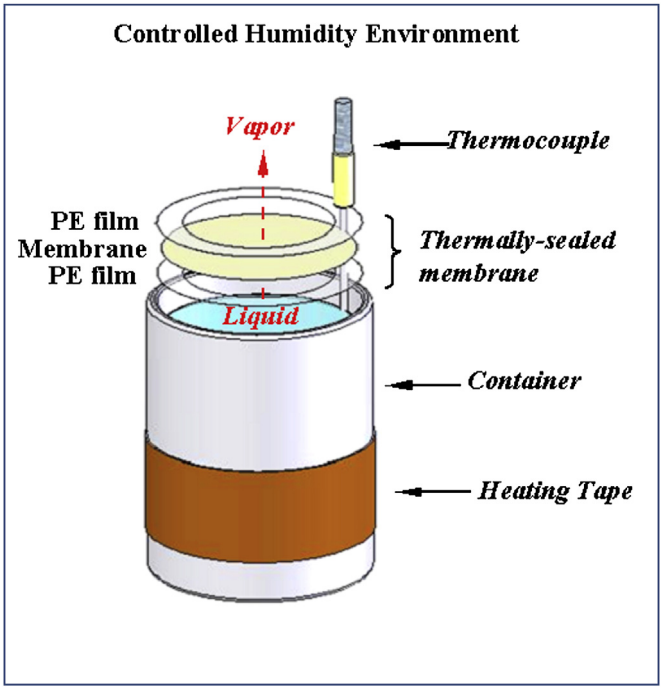

Fig. 1. Schematic diagram of liquid–vapor permeation (LVP) measurement apparatus.

Table 1
ECSA and double-layer capacitances (C_{dl}) at 80 °C and 80% RH.[a]

Membranes	ECSA (H-des) ($m^2\ g^{-1}$)	ECSA (H-ads) ($m^2\ g^{-1}$)	ECSA[b] ($m^2\ g^{-1}$)	C_{dl} (mF cm^{-2})
NRE-211	62.4 ± 2.7	60.0 ± 2.8	61.2 ± 2.7	58.0 ± 0.9
SSC-1.30	63.2 ± 1.1	65.7 ± 2.0	64.5 ± 1.7	60.6 ± 1.3
SSC-1.37	66.4 ± 3.5	61.8 ± 3.4	64.1 ± 3.5	58.0 ± 0.2
SSC-1.43	61.7 ± 2.5	65.0 ± 3.3	63.3 ± 2.7	59.5 ± 0.1
SSC-1.50	63.8 ± 3.2	65.4 ± 1.1	64.6 ± 2.4	61.3 ± 1.8

[a] Data refers to the cathode layer of MEAs.
[b] Average of ECSA (H-des) and ECSA (H-ads).

The differential chemical potential across the membrane constitutes the driving force responsible for water permeation through the membrane. Values of the permeation coefficient (permeance), expressed as a function of chemical potential, were obtained from the slopes of plots of the water fluxes against chemical potential difference. Normalizing these values to thickness of the hydrated membrane provided the water permeability values. The details of this calculation are described in our previous work [29,30]. The errors reported are based on multiple (3) measurements.

3. Results and discussion

3.1. Fuel cell performance

The electrochemically active surface area (ECSA) of platinum catalyst in the cathode was estimated using cyclic voltammetry. ECSA data and double-layer capacitances (C_{dl}) at 80 °C and 80% RH are presented in Table 1 for the catalyst-coated membranes. The average ECSA and C_{dl} values were similar for all samples, between 61.3–63.6 $m^2\ g^{-1}$ and 57.4–63.5 mF cm^{-2}, respectively, indicating that the contact area between Pt and Nafion ionomer is similar for all membranes studied, and confirms that the parameter being varied in this work is solely the membrane and not the catalyst layer.

Three pieces of NRE-211 membrane were used to establish the reproducibility of the MEA fabrication and testing procedures. Averaged polarization curves, obtained under different relative humidities at a cell temperature at 80 °C, for NRE-211- and SSC PFSA-based single cells are presented in Figs. 2 and 3 and Figure S1 (supporting information). Under conditions of 80 °C and 80% RH (Fig. 2) the fuel cell polarization curves for SSC PFSA and NRE-211

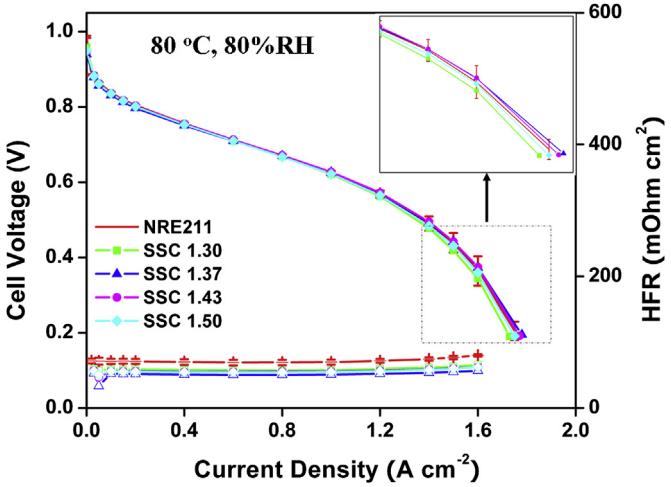

Fig. 2. Cell voltage and high frequency resistance as function of current density for NRE-211 and SSC membranes at 80 °C and 80% RH.

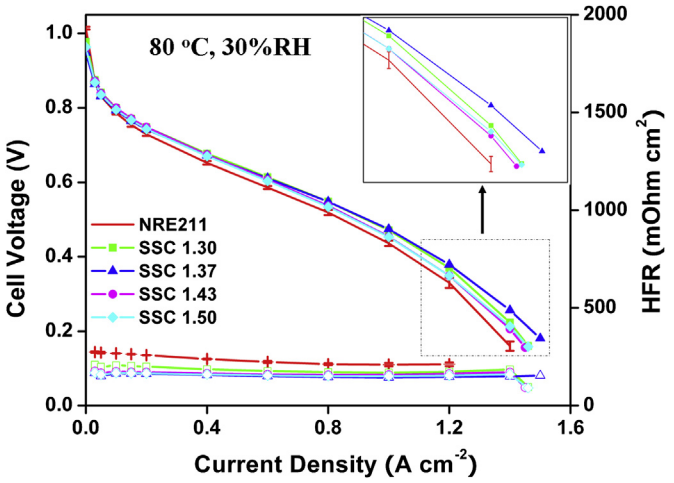

Fig. 3. Cell voltage and high frequency resistance as function of current density for NRE-211 and SSC membranes at 80 °C and 30% RH.

membranes are almost identical indicating a difference in potential of <10 mV at 1.2 A cm^{-2}. In contrast, SSC PFSA-based cells consistently provided higher performance than NRE-211-based cells under lower RH operation (see Fig. 3 and Figure S1). In particular, at 80 °C and 30% RH operation, the cell voltages of SSC PFSA membrane cells were significantly higher (see Fig. 3) – for example, the potential of SSC PFSA-1.37-based cells was 379 mV at 1.2 A cm^{-2}, compared to 330 mV for NRE-211.

H_2/air polarization curves and HFR data were obtained at an elevated temperature of 95 °C and various relative humidities (see supporting information, Figures S2–S4.) The same trend was observed as above: increasingly higher relative performance was observed for SSC PFSA-based cells as RH was decreased. This is more apparent when the RH was <50%. For example, under 30% RH a potential of 347 mV was generated for SSC PFSA-1.37 cells at 1.2 A cm^{-2} in comparison to 254 mV for NRE-211-based cells, representing to a 37% difference in power output. Of the three PFSA SSC membranes investigated, SSC-1.37 displayed the highest power density under low RH operation (0.46 W cm^{-2}, see Figure S5), the reasons for which are discussed in the next section.

Using HFR data, IR-compensated H_2/air polarization curves were calculated, as shown in Fig. 4 and Figure S6. The data lie on a common curve for a given set of temperature and RH conditions, revealing that the higher performance of SSC PFSA membranes over NRE-211 can be attributed to their lower HFR. The high frequency resistance (HFR) and conductivities calculated from HFRs of SSC PFSA- and NRE-211-based cells are shown in Figures S7 and S8, Table 2 and Fig. 5. For all cells investigated, SSC PFSA-based cells yielded lower HFR and higher conductivities relative to NRE-211-based cells under all investigated current densities and fuel cell operating conditions.

SSC PFSA membranes exhibit a minimum HFR value and a corresponding maximum conductivity for IEC 1.37 meq g^{-1}. As the RH is reduced, HFR values increase but are still lower in value than SSC PFSA-based cells. The difference in HFR between SSC PFSA-based cells and NRE-211-based cells increases with decreasing RH. For example, the HFR at 1 A cm^{-2} under 80% RH was 2.03 mΩ, and 2.78 mΩ for SSC PFSA-1.37 and NRE-211-based cells, respectively. When the RH is decreased from 80% to 30%, the difference in HFR between the two cells increased from 0.75 mΩ to 2.82 mΩ. In addition, HFR values decreased as the current density increased and the difference in HFR increased with decreasing RH.

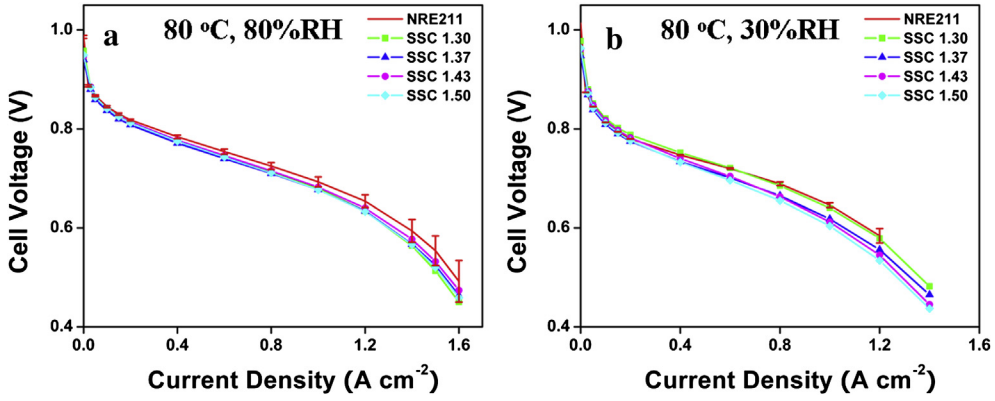

Fig. 4. IR-compensated H_2/air polarization curves (a) at 80 °C and 80% RH and (b) at 80 °C and 30% RH.

Table 2
Ohmic resistance and relative conductivity calculated from HFR at 0.03 A cm^{-2} and 1 A cm^{-2} under different fuel cell operating conditions.

	NRE-211	SSC-1.30	SSC-1.37	SSC-1.43	SSC-1.50
Wet thickness (μm)	28	28	24	23	24
80 °C, 80% RH					
HFR (mΩ) at 0.03 A cm^{-2}	2.86 ± 0.08	2.38 ± 0.07	2.11 ± 0.10	2.28 ± 0.08	2.25 ± 0.09
σ_{HFR} (S cm^{-1}) at 0.03 A cm^{-2}	0.038 ± 0.001	0.044 ± 0.001	0.045 ± 0.002	0.042 ± 0.001	0.041 ± 0.002
HFR (mΩ) at 1 A cm^{-2}	2.78 ± 0.05	2.30 ± 0.07	2.03 ± 0.04	2.21 ± 0.04	2.20 ± 0.04
σ_{HFR} (S cm^{-1}) at 1 A cm^{-2}	0.039 ± 0.001	0.045 ± 0.001	0.047 ± 0.001	0.043 ± 0.001	0.042 ± 0.001
80 °C, 30% RH					
HFR (mΩ) at 0.03 A cm^{-2}	10.98 ± 0.09	8.37 ± 0.08	6.69 ± 0.07	7.06 ± 0.08	6.75 ± 0.09
σ_{HFR} (S cm^{-1}) at 0.03 A cm^{-2}	0.010 ± 0.0001	0.012 ± 0.0001	0.014 ± 0.0001	0.013 ± 0.0002	0.013 ± 0.0002
HFR (mΩ) at 1 A cm^{-2}	8.60 ± 0.02	6.77 ± 0.01	5.78 ± 0.01	6.31 ± 0.01	6.04 ± 0.008
σ_{HFR} (S cm^{-1}) at 1 A cm^{-2}	0.012 ± 0.0001	0.015 ± 0.0001	0.017 ± 0.0001	0.015 ± 0.0001	0.015 ± 0.0001

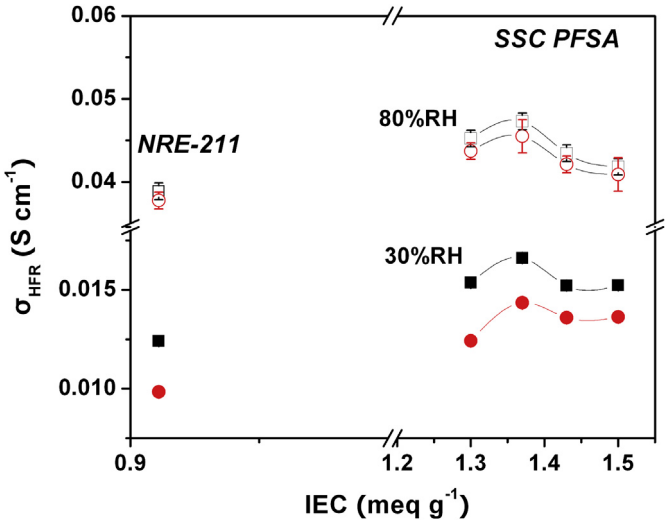

Fig. 5. Conductivities calculated from HFR at 0.03 A cm^{-2} (circle) and at 1 A cm^{-2} (square) as a function of IEC under 80% RH (open) and 30% RH, at 80 °C (solid).

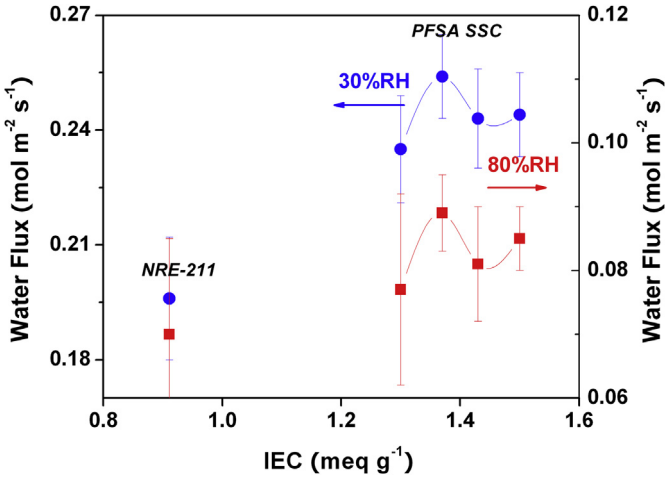

Fig. 6. Liquid–vapor water fluxes of SSC and NRE-211 for liquid/80% RH (square) and liquid/30% RH (circle) conditions as a function of IEC, at 80 °C.

3.2. Water permeation

For liquid–vapor permeation (LVP) measurements, the membrane was exposed to liquid water on one side and water vapor on the other. A water concentration gradient develops across the membrane which serves to drive water transport from the liquid side to the vapor side. The rates of water flux through SSC membranes compared with NRE-211 are shown in Fig. 6 and listed in Table 3. The LVP water fluxes

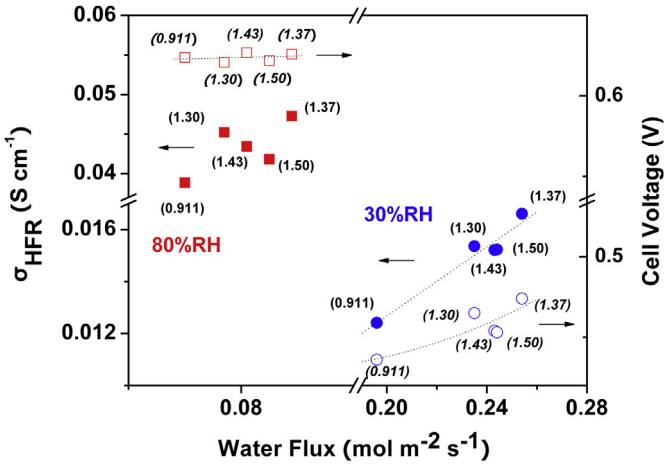

Fig. 7. σ_{HFR} (solid) and cell voltages (void) at 1 A cm^{-2} for SSC PFSA- and NRE-211-based cells at 80% RH (square) and 30% (circle), as a function of water fluxes, at 80 °C.

of the membranes at 80 °C and 30% RH on the vapor side were ~three times larger than those at 80 °C and 80% RH as a result of the higher driving force constituted by the larger chemical potential difference of water across the membrane. For example, the water fluxes of SSC PFSA-1.37 were 0.254 mol m^{-2} s^{-1} for liquid/30% RH, compared to 0.089 mol m^{-2} s^{-1} under liquid/80% RH conditions. Furthermore, the difference in water flux between SSC PFSA and NRE-211 increased with decreasing RH. For example, the water fluxes at 80 °C and liquid/80% RH operation was 0.089 mol m^{-2} s^{-1}, and 0.070 mol m^{-2} s^{-1} for SSC PFSA-1.37 and NRE-211, respectively. When the RH is decreased from liquid/80% to liquid/30%, the difference in water fluxes between the two membranes increased from 0.058 mol m^{-2} s^{-1} to 0.19 mol m^{-2} s^{-1}.

The water fluxes are normalized for thickness, first by converting the data to permeance, and then by multiplying permeance by membrane thickness to provide permeability (see Table 3). In general, the water fluxes for SSC PFSA membranes are larger than NRE-211 under both liquid/RH 80% and liquid/RH 30% (see Fig. 6). However the permeabilities are similar for liquid/80% RH conditions, and marginally larger for SSC membranes compared to NRE-211 liquid/30% RH. This is because the membranes examined are relatively thin (~20 μm), and water transport resistance across the vapor–membrane interface plays an increasingly large role in determining the overall water flux for thin membranes.

3.3. Discussion

When current is drawn from a fuel cell, water is generated electrochemically at the cathode. Protons diffusing from anode to cathode "drag" water by electro-osmosis. Under moderate to high current loads, the cathode side of the MEA is exposed to liquid water while the anode experiences drier conditions. Measurement

Table 3
LVP water transport through membranes at 80 °C: liquid/80% RH and liquid/30% RH.

	NRE-211	SSC-1.30	SSC-1.37	SSC-1.43	SSC-1.50
Wet thickness (μm)	28	28	24	23	24
Liquid/80% RH					
Water flux (× 10^{-1} mol m^{-2} s^{-1})	0.70 ± 0.15	0.77 ± 0.15	0.89 ± 0.06	0.81 ± 0.09	0.85 ± 0.05
Permeance (× 10^{-9} mol Pa^{-1} m^{-2} s^{-1})	1.52 ± 0.33	1.66 ± 0.33	1.92 ± 0.09	1.75 ± 0.19	1.83 ± 0.10
Permeability (× 10^{-14} mol Pa^{-1} m^{-1} s^{-1})	4.27 ± 0.95	4.66 ± 0.91	4.41 ± 0.31	4.03 ± 0.46	4.39 ± 0.25
Liquid/30% RH					
Water flux (× 10^{-1} mol m^{-2} s^{-1})	1.96 ± 0.16	2.35 ± 0.14	2.54 ± 0.11	2.43 ± 0.13	2.44 ± 0.11
Permeance (× 10^{-9} mol Pa^{-1} m^{-2} s^{-1})	0.95 ± 0.07	1.14 ± 0.07	1.23 ± 0.05	1.18 ± 0.06	1.18 ± 0.05
Permeability (× 10^{-14} mol Pa^{-1} m^{-1} s^{-1})	2.66 ± 0.22	3.19 ± 0.19	2.84 ± 0.12	2.71 ± 0.14	2.83 ± 0.12

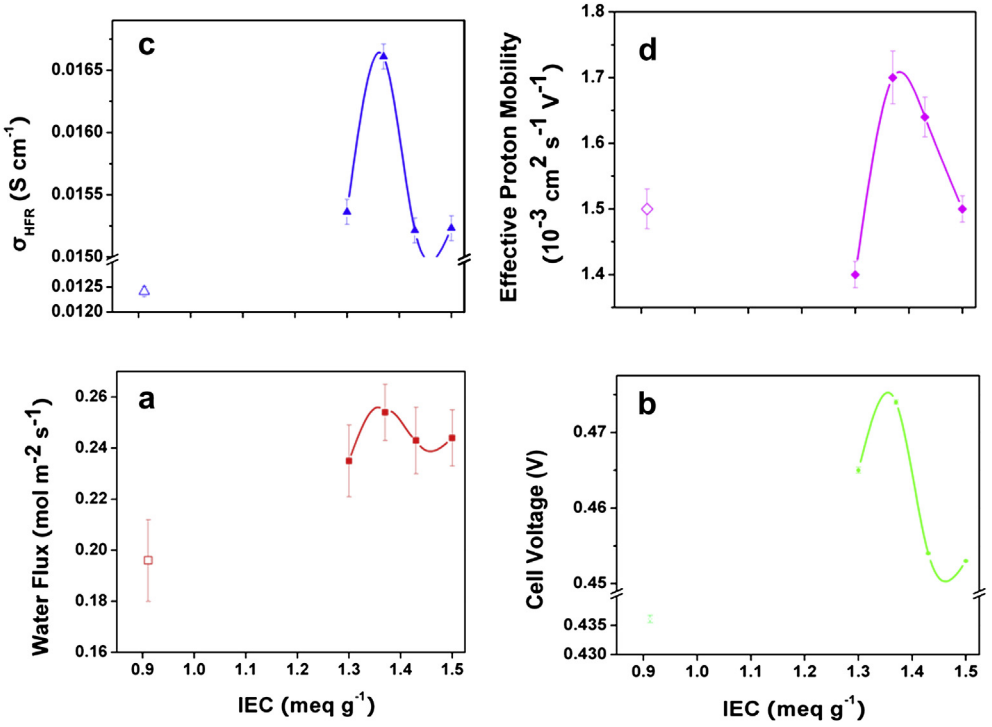

Fig. 8. (a) Water flux, (b) cell voltage at 1 A cm^{-2}, (c) σ_{HFR}, 30% RH and (d) effective proton mobility as a function of IEC. Temperature, 80 °C.

of water permeation, such as described in this work, provides a reasonable facsimile for fuel cell operating conditions [29]. It is therefore pertinent to examine the relationship between water transport properties and fuel cell performance data. In Fig. 7, we plot σ_{HFR} and the cell voltage at 1 A cm^{-2} as function of water flux. A linear relationship between water flux and σ_{HFR} under drier conditions of 80 °C and 30% RH is observed. Furthermore, under relatively "drier" conditions of 80 °C and 30% RH the difference in water flux correlates strongly with cell voltage. We believe this is because the membranes are less hydrated under 30% RH and that differences in water transport through membranes have a stronger influence on σ_{HFR} under these low RH conditions. Under relatively high humidity, 80% RH, the water flux also impacts σ_{HFR}, but the correlation between water flux and σ_{HFR} is not as strong. Moreover, under 80% RH the water flux does not affect the cell voltage as significantly because the membranes are sufficiently hydrated and differences in water transport across the membranes under these conditions do not substantially impact their hydration level and hence fuel cell performance.

The relationship between fuel cell performance, σ_{HFR}, water flux and IEC (at 80 °C and 30% RH) is further illustrated in Fig. 8a–c. The cell voltage, σ_{HFR} and water flux show a similar trend of exhibiting a maximum at IEC 1.37 meq g^{-1}. In an attempt to explain why PFSA SSC series membranes exhibit a maximum at 1.37 meq g^{-1} we examined another transport property of the membranes the *effective* proton mobility, μ'_{H^+}, which was calculated using Eq. (5), [31] (see supporting information, Table S1):

$$\sigma_{H^+} = F[-SO_3H]\mu'_{H^+} \quad (5)$$

where σ_{H^+} is the proton conductivity; *F*, the Faraday constant; and [−SO$_3$H], the volumetric acid concentration. As can be observed from Fig. 8d, a volcano-type curve is also observed for a plot of μ'_{H^+} vs IEC. It is not surprising that water contents of SSC membranes increase with increasing IEC (see supporting information, Figure S9), and consequently, due to dilution effects, [−SO$_3$H] decreases with IEC. What is surprising however is that the effective proton mobility shows a maximum series at 1.37 meq g^{-1} and decreases on further increases in IEC; this, despite the fact that the water content increases, which should serve to promote proton mobility. This counter-intuitive observation has been made previously by Luo et al. [26], who showed that the connectivity of the hydrophilic network is not as well developed in high IEC SSC PFSA membranes, and that the additional water volume sorbed by increasing the IEC is not fully utilized due to an increasing number of 'dead-ends.' A similar trend in the relationship between the cell voltage and water flux as function of IEC is observed in the present work and is interpreted as resulting from water and protons transporting through the same tortuous paths.

4. Conclusion

Short-side chain PFSA membranes (IEC 1.30, 1.37, 1.43, 1.50 meq g^{-1}) showed higher fuel cell performance than NRE-211 at 80 °C and 30% RH. PFSA SSC-1.37 provided the highest performance within the limited selection of membranes studied. This membrane also provided the highest rate of water permeation and proton mobility. The following conclusions are drawn:

1. A higher rate of water flux through membranes is a factor that contributes to improving the fuel cell performance under "dry" conditions. This is because the increased rate of water transport serves to offset the under-hydration state the membranes experience for low RH conditions. Under relatively high RH fuel cell conditions, the influence of differences in water transport between membranes on fuel cell performance is less significant because the membranes are more fully hydrated in the first instance.
2. Rates of water permeation and effective proton mobility are inherently linked since water molecules and protons travel through the same tortuous, hydrophilic channels.

3. While increasing the IEC of membranes is accompanied by an increase in water content, this does not necessarily lead to an increase in water transport and effective proton mobility; these are determined by the polymer architecture, ionic aggregation and polymer-polymer interactions that dictate the membrane's morphology. As such, simply increasing the membrane's IEC may not improve higher fuel cell performance under "dry" conditions.

Acknowledgement

We gratefully acknowledge Dongyue Group Co. Ltd. for synthesis of the SSC PFSA ionomers and Automotive Fuel Cell Cooperation Corp. (AFCC) for partially financial support.

Appendix A. Supplementary material

Supplementary material associated with this article can be found, in the online version, at http://dx.doi.org/10.1016/j.jpowsour.2013.05.176.

References

[1] P.P. Kundu, A. Pal, Rev. Chem. Eng. 22 (2006) 125–153.
[2] K.D. Kreuer, Chem. Phys. Chem. 3 (2002) 771–775.
[3] E.E. Boakye, H.L. Yeager, J. Membr. Sci. 69 (1992) 155–167.
[4] M.R. Tant, K.D. Lee, K.P. Darst, C.W. Martin, Polym. Mater. Sci. Eng. 58 (1988) 1074–1078.
[5] M.R. Tant, K.P. Darst, K.D. Lee, C.W. Martin, ACS Symp. Ser. 395 (1989) 370–400.
[6] R.B. Moore, C.R. Martin, Macromolecules 22 (1989) 3594–3599.
[7] K. Prater, J. Power Sources 29 (1990) 239–250.
[8] M.G. De Angelis, S. Lodge, M. Giacinti Baschetti, G.C. Sarti, F. Doghieri, A. Sanguineti, P. Fossati, Desalination 193 (2006) 398–404.
[9] L. Merlo, A. Ghielmi, L. Cirillo, M. Gebert, V. Arcella, J. Power Sources 171 (2007) 140–147.
[10] K.D. Kreuer, M. Schuster, B. Obliers, O. Diat, U. Traub, A. Fuchs, U. Klock, S.J. Paddison, J. Maier, J. Power Sources 178 (2008) 499–509.
[11] D. Gorri, M.G. De Angelis, M. Giacinti Baschetti, G.C. Sarti, J. Membr. Sci. 322 (2008) 383–391.
[12] D.S. Wu, S.J. Paddison, J.A. Elliott, Macromolecules 42 (2009) 3358–3367.
[13] A.S. Aricò, A. Di Blasi, G. Brunaccini, F. Sergi, G. Dispenza, L. Andaloro, M. Ferraro, V. Antonucci, P. Asher, S. Buche, D. Fongalland, G.A. Hards, J.D.B. Sharman, A. Bayer, G. Heinz, N. Zandonà, R. Zuber, M. Gebert, M. Corasaniti, A. Ghielmi, D.J. Jones, Fuel Cells 10 (2010) 1013–1023.
[14] A. Stassi, I. Gatto, E. Passalacqua, V. Antonucci, A.S. Arico, L. Merlo, C. Oldani, E. Pagano, J. Power Sources 196 (2011) 8925–8930.
[15] V. Arcella, C. Troglia, A. Ghielmi, Ind. Eng. Chem. Res. 44 (2005) 7646–7651.
[16] A. Ghielmi, P. Vaccarono, C. Troglia, V. Arcella, J. Power Sources 145 (2005) 108–115.
[17] I.H. Hristov, S.J. Paddison, R. Paul, J. Phys. Chem. B 112 (2008) 2937–2949.
[18] J. Peron, D. Edwards, M. Haldane, X.Y. Luo, Y.M. Zhang, S. Holdcroft, Z.Q. Shi, J. Power Sources 196 (2011) 179–181.
[19] C. Lei, D. Bessarabov, S. Ye, Z. Xie, S. Holdcroft, T. Navessin, J. Power Sources 196 (2011) 6168–6176.
[20] J.S. Yi, T.V. Nguyen, J. Electrochem. Soc. 145 (1998) 1149–1998.
[21] S.H. Ge, X.G. Li, B.L. Yi, I.M. Hsing, J. Electrochem. Soc. 152 (2005) A1149–A1157.
[22] M. Eikerling, Y. Kharkats, A.A. Kornyshev, Y. Volfkovich, J. Electrochem. Soc. 145 (1998) 2684–2699.
[23] M. Eikerling, J. Electrochem. Soc. 153 (2006) E58–E70.
[24] H.A. Gasteiger, W. Gu, R. Makihara, M.F. Mathias, B. Sompalli, Beginning-of-life MEA performance — efficiency loss contributions, in: W. Vielstich, A. Lamm, H.A. Gasteiger (Eds.), Handbook of Fuel Cells, John Wiley & Sons Ltd., West Sussex, 2003, p. 593.
[25] V. Arcella, A. Ghielmi, G. Tommasi, Ann. N.Y. Acad. Sci. 984 (2003) 226–244.
[26] X.Y. Luo, S. Holdcroft, A. Mani, Y.M. Zhang, Z.Q. Shi, Phys. Chem. Chem. Phys. 13 (2011) 18055–18062.
[27] Z. Xie, X. Zhao, M. Adachi, Z. Shi, T. Mashio, A. Ohma, K. Shinohara, S. Holdcroft, T. Navessin, Energy Environ. Sci. 1 (2008) 184–193.
[28] T.J. Peckham, J. Schmeisser, S. Holdcroft, J. Phys. Chem. B 112 (2008) 2848–2858.
[29] M. Adachi, T. Navessin, Z. Xie, B. Frisken, S. Holdcroft, J. Electrochem. Soc. 156 (2009) B782–B790.
[30] M. Adachi, T. Navessin, Z. Xie, F.H. Li, S. Tanaka, S. Holdcroft, J. Membr. Sci. 364 (2010) 183–193.
[31] T.J. Peckham, J. Schmeisser, M. Rodgers, S. Holdcroft, J. Mater. Chem. 17 (2007) 3255–3268.